Lithium metal-mediated electrochemical degradation of per- and poly-fluoroalkylsubstances (PFAS)

Bidushi Sarkar[1], Rameshwar L. Kumawat[2], Peiyuan Ma[1], Ke-Hsin Wang[1], Matin Mohebi[1], George C. Schatz[2], and Chibueze V. Amanchukwu[1]*

[1]Pritzker School of Molecular Engineering, The University of Chicago, Chicago, IL 60637 USA

[2]Department of Chemistry, Northwestern University, Evanston, IL 60208, USA

*Corresponding author

Email: chibueze@uchicago.edu

Abstract

Per- and poly-fluoroalkyl substances (PFAS) have significant environmental and health hazards. Unfortunately, current PFAS degradation routes require higher temperatures or highly corrosive conditions and/or lead to incomplete defluorination and generation of shorter alkyl chains. Fortunately, fluorinated compounds are highly vulnerable to reduction. Inspired by the lithium metal battery literature, we develop an ambient temperature and pressure electrochemical degradation process that takes advantage of reactive metals and highly reducing environments. We show that electrodeposited lithium metal can enable 95% degradation and 94% defluorination of a long chain PFAS, perfluorooctanoic acid (PFOA) without forming any shorter C_2-C_7 PFAS as end products. More importantly, we show mineralization to LiF. Using density functional theory (DFT) and ab initio molecular dynamics (AIMD), we reveal the degradation mechanism and show that electron transfer from Li to PFOA leads to rapid C-F bond cleavage, the formation of fluoride, and carbon chain fragments. We expand the scope to other PFAS compounds and of the 33 PFAS compounds tested, 22 demonstrated degradation amounts exceeding 70% (with some degradation up to 99%), and complete mineralization to inorganic fluorides. Finally, we use the mineralized F^- as a fluorine source for the synthesis of fluorinated non-PFAS compound such as ethane sulfonyl fluoride to complete a circular fluorine loop from waste to valuable product. Our work showcases a novel electrochemical approach that borrows from the battery literature to solve challenges in environmental remediation.

Introduction

Per- and poly- fluoroalkyl substances (PFAS) are a class of thousands of man-made chemicals that are ubiquitously used in consumer and industrial applications.[1] These contain at least one perfluorinated carbon (-CF_3 or -CF_2 with no H) and have a wide range of special properties such as high chemical stability, water resistance, and more. Unfortunately, they are persistent in the environment and are colloquially known as 'forever chemicals.'[2] Furthermore, they have been implicated in a wide range of health-related concerns including cancer and immune impairment.[3, 4] Therefore, across the world, new regulations have been proposed or implemented to curtail their use and limit their concentration in drinking water.[5] Addressing the PFAS challenge requires sensing, capture, and destruction. There are many sensing approaches based on nanotechnology, biotechnology etc. that have been developed to sense PFAS compounds at concentrations as low as 1 ppt.[6, 7] Furthermore, carbon, and other sorbents can capture a range of PFAS compounds.[8-10] However, there are limited approaches to permanently degrade and mineralize these PFAS compounds to fluoride.

PFAS degradation is of utmost importance because many of the environmental and health exposures are a result of improper disposal and limited degradation technologies. Degradation approaches have lagged because of the strength of the C-F bond. Several approaches such as thermal, photo, chemical, and electrochemical approaches to PFAS destruction have been studied.[11-13] Perfluorooctanoic acid (PFOA) is one pollutant of great interest as it is ranked among the US EPA (Environmental Protection Agency) top 10 and consistently observed in the environment and in almost all humans.[14] In addition, there are several legacy and current PFAS compounds in wide production.

Electrochemical approaches are of great interest because they can be done under ambient temperature and pressure conditions and take advantage of renewable electrons from solar and wind.[15] Electrochemical oxidation – not reduction – has been heavily explored. Electrodes such as boron doped diamond (BDD) are state-of-the-art for electrochemical oxidation and are primarily used not because it is an active catalyst for PFAS degradation but because it has a high overpotential for oxygen evolution.[16, 17] Hence, when electrochemical oxidation is performed under aqueous conditions, the higher potentials required for PFAS oxidation can be accessed. Unfortunately, BDD is very expensive.[18]

Fluorine is the most electronegative element known. Therefore, C-F bonds are highly resistant to oxidation. In contrast, fluorinated compounds are vulnerable to reduction. In the field of nonaqueous batteries such as lithium metal, fluorinated solvents and salts are state-of-the-art due to their non-flammability, high thermal resistance, and oxidative stability.[19, 20] At reductive conditions and/or in contact with reactive metals such as lithium or sodium, these compounds are known to degrade to form the solid electrolyte interface.[21] Chemical and surface characterization techniques show mineralization to F^-.[22] Furthermore, these reactive metals can corrode at rest upon contact with these fluorinated solvents.[23] In In the battery literature, continuous reactivity between the fluorinated electrolyte and the metal electrode is highly undesired and leads to poor battery cycling.[24, 25] However, this is exactly what is desired for PFAS degradation! *Therefore, the challenges of fluorinated electrolyte instability and reaction that plague metal batteries open a new approach and opportunity for pollutant degradation*.

Inspired by the lithium metal battery[21, 26, 27] and lithium mediated ammonia synthesis literature,[28, 29] we propose the investigation of PFAS degradation under reductive conditions

and in the presence of a reactive metal. There are fewer studies on electrochemical reduction of PFAS that take advantage of the inherent reductive vulnerability of fluorinated compounds. The generation of aqueous electrons (*aq* e-) for reductive degradation of PFAS in water typically requires complex and energy-intensive methods such as plasma discharge, UV irradiation or radiolysis.[30] A major challenge is that these *aq* e- are highly reactive and can be easily scavenged by H^+ or O_2 present in the water. This scavenging effect significantly limits the availability of *aq* e- for effective PFAS degradation and often necessitates the use of anaerobic conditions to mitigate this issue.[31] We speculate that another reason for the dearth in the literature is that if the reduction reaction is performed under aqueous conditions, the hydrogen evolution reaction (HER) would occur before the potentials needed for PFAS reduction.[32] In addition, reactive metals such as lithium and sodium react violently with water. However, while PFAS is often present in the environment in water or in soil, it can be captured, concentrated and then destroyed in a different media. Therefore, to take advantage of reactive metals and reduction potentials for PFAS degradation requires nonaqueous electrolytes.

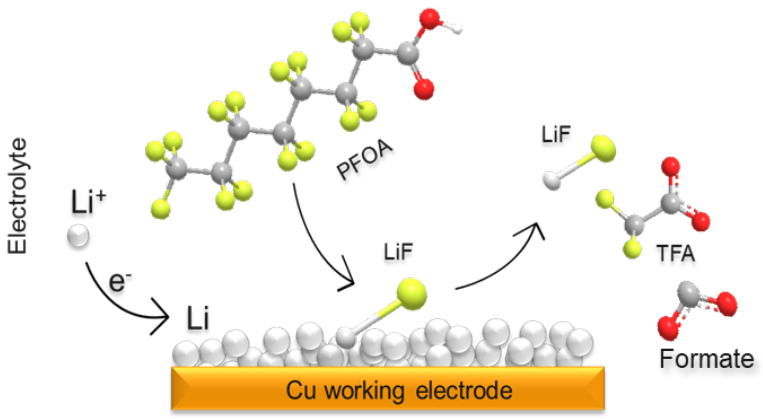

Figure 1. Schematic of the proposed Li mediated PFOA degradation approach.

There have been some papers that explored the influence of nonaqueous solvents on PFAS degradation. McCord et al. showed that different nonaqueous solvents such as dimethyl sulfoxide (DMSO) facilitate the decarboxylation of PFOA, which is often reported as the gateway to degradation.[33] Dichtel et al. used 30 M NaOH dissolved in a DMSO/water mixture and showed that at elevated temperatures (120°C), decarboxylation can occur with subsequent defluorination to fluoride.[34] However, high temperatures are required, at least for the initial decarboxylation step. Additionally, a highly corrosive NaOH electrolyte is necessary. Liu et al. demonstrated PFOA degradation into shorter alkyl chains in aprotic solvents like N-N-dimethylformamide and acetonitrile using a Rh/Ni cathode.[35] However, a reductive metal mediated electrochemical method to degrade PFOA to inorganic fluorides at ambient conditions without generating smaller chain PFAS remains unknown. While it is important to degrade PFAS compounds, it is important to note that fluorine has been listed as a critical element by the Department of Energy.[36] Furthermore, there are numerous fluorinated compounds that are not classified as PFAS. Therefore, mineralizing PFAS to F^- and valorizing the F^- to synthesize non-PFAS fluorinated compounds would enable a circular fluorine economy and upcycling to valuable products.

In this work, we develop a reactive metal-assisted degradation *via* electroreduction (ReMADE) process for the remediation of halogenated compounds (**Figure 1**). The process occurs at ambient temperature and pressure in a single chamber membrane-and-catalyst-free electrochemical cell. We show that upon lithium metal electrodeposition, up to 95% PFOA degradation and 94% defluorination can be achieved. More importantly, we reveal that no short chain PFAS compounds are formed and almost complete mineralization to fluoride is achieved. Our findings showcase a new process for the efficient and selective degradation of PFAS deeply inspired by the lithium metal battery literature. We use the confluence of DFT (density functional theory), AIMD (ab initio molecular dynamics), and spectroscopic tools to understand the degradation mechanism. We also expand the ReMADE process scope by probing other reactive metals and other PFAS compounds. Finally, we use the F^- obtained from PFAS degradation as the fluorine source for the synthesis of a non-PFAS fluorinated compound (ethane sulfonyl fluoride, ESF) that has seen applications as an additive or solvent for batteries as well as for pharmaceuticals.[37, 38] The ReMADE process cleverly takes advantage of the degradation challenges that batteries face and unleashes them for other electrochemical transformations such as electrosynthesis, electrocatalysis, and environmental remediation.

Results and discussion

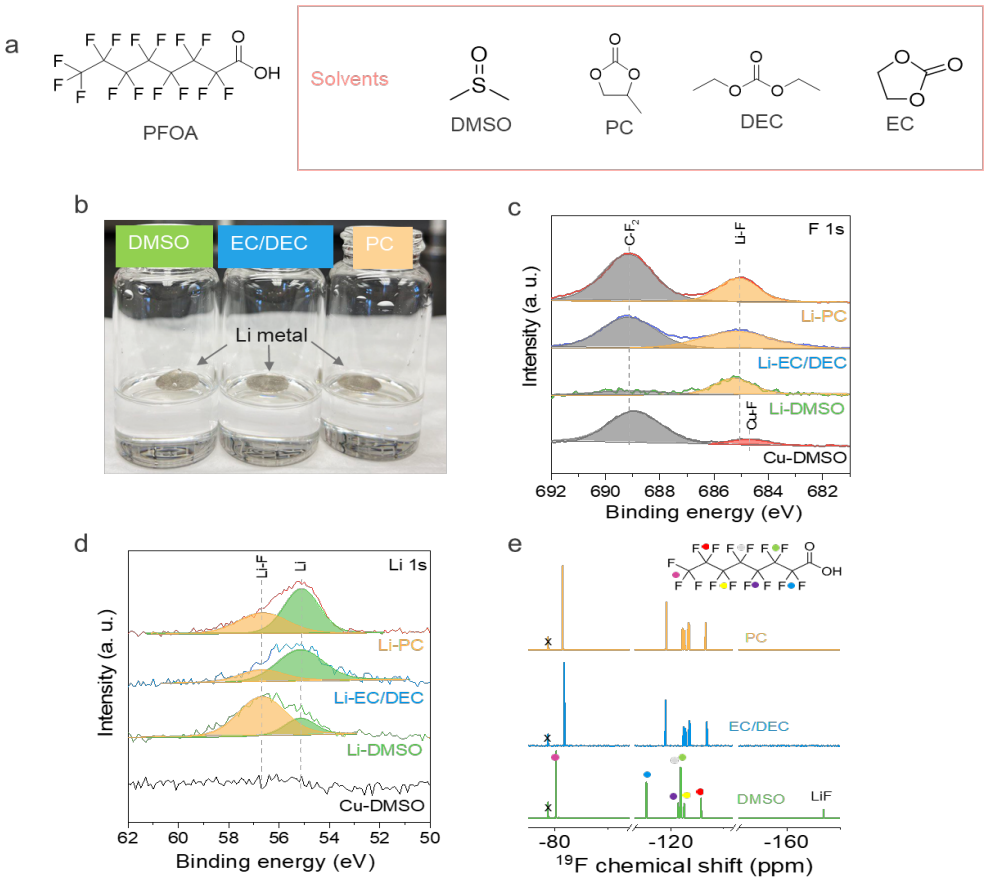

Fig 2. Proof-of-concept chemical reaction between PFOA and Li. (**a**) Structure of PFOA, and different solvents tested for PFOA degradation, (**b**) Image of Li metal in different solvents containing PFOA, (**c**) F 1s and (**d**) Li 1s HRXPS of Li metal in different solvents containing PFOA, and (**e**) ^{19}F NMR of fluorinated compounds after exposure of lithium metal to PFOA in different solvents after 24 h. Cross (x) denotes the internal standard LiTFSI.

Rationale for process and proof-of-concept

The reactivity of 'reactive' metals such as lithium towards PFOA was first studied chemically. We focus on PFOA as it is the most prevalent of PFAS compounds. Lithium metal was added to a solution containing 10 mM of dissolved PFOA. As **Figure 1 (a)** shows, we choose solvents such as dimethyl sulfoxide (DMSO), ethers, and carbonates that are relatively stable against lithium metal and have been studied in the lithium metal battery literature.[39-42] In contrast, acetonitrile reacts violently with lithium metal and was not explored.[43] After 24 hours of exposure of the lithium metal piece to PFOA in the different solvents (**Figure 1 (b)**), the lithium metal surface was studied using XPS. Across all the solvents studied, mineralization to LiF was observed as shown in the F 1s XPS (**Figure 1 (c, d)**).[44, 45] A Cu foil was also examined in DMSO as a control that shows the presence of C-F_2 and Cu-F peak[46] indicating that these interactions are arising by residual PFOA on the surface. Residual PFOA can also be seen at the lithium surface for the carbonate-based solvents. For DMSO, it appears that the fraction of LiF seen is much higher compared to the other solvents.

The supernatant was also studied using ^{19}F solution NMR (**Figure 1 (e)**). Interestingly, dissolved LiF was also observed when DMSO is used as the solvent. We assign the fluoride peak at 166.6 ppm following a LiF in DMSO control (**Figure S1**). There were no observations of smaller chain fluorinated compounds. Although the XPS data in other aprotic solvents like EC/DEC and PC show LiF formation, there is no observation of F^- in solution. We attribute this to lower LiF solubility in carbonate solvents compared to DMSO and the absolute lower amount of LiF formed (as seen in the XPS data).[47, 48] The combination of XPS and NMR irrefutably show that reactive metals such as lithium can enable PFOA degradation and mineralization to fluoride. However, as a surface driven reaction, fresh new lithium metal surface will always be needed. Therefore, an electrochemical process was developed.

Electrochemical degradation of PFOA

An ambient temperature, pressure, electrochemical process was developed to enhance PFAS degradation. As **Figure S2** shows, the electrochemical cell consists of an organic solvent, dissolved salt, a Cu working electrode, a Pt or graphite counter electrode, and an Ag/Ag^+ leakless reference electrode. For lithium metal batteries, fluorinated salts such as LiFSI (lithium bis(fluorosulfonyl)imide) and LiTFSI (lithium bis(trifluoromethane)sulfonimide) are state-of-the-art as they have been shown to enable high Coulombic efficiencies (stripping capacity/deposition capacity).[37] However, since we are interested in PFOA degradation, we avoid any other fluorine source. Hence, salts such as ClO_4^- and NO_3^- were studied. These salts limit the type of solvents that can be explored to ensure sufficient salt dissolution and high ionic conductivity. Hence, a range of electrolytes were explored and compositions that yielded ionic conductivities > 3 mS/cm were studied (**Table S1**). Regardless, an interesting philosophical question that guides the proposed approaches and distinguishes it starkly from lithium metal batteries: do we want electrolytes that support high lithium metal Coulombic efficiency or not? High CE electrolytes often have low surface area and limited reaction with lithium metal. However, we do want large surface area and greater reactivity with PFAS. Hence, the guiding principles for lithium metal batteries will differ from reactive metal mediated reactions.

First, $TBAClO_4$ (tetrabutylammonium perchlorate) salt was used to ascertain the impact of the applied potential and current density by direct electroreduction (DE) without the presence of lithium. Using a current density of 50 mA/cm^2 with a catalyst-free Cu working electrode, significant degradation of PFOA and mineralization to F^- is observed at ambient conditions (**Figure 3**). Using a combination of a fluoride ion selective electrode (ISE, **Supplementary note 1**) and ^{19}F NMR (**Supplementary note 2**), over 69 % of PFOA degrades and 70 % defluorination occurs to F^-. This observation further reinforces the promise of reductive potentials for dehalogenation reactions in contrast to conventional oxidative processes that are used. Jiang et al. also recently explored a molecular catalyst for reductive PFAS degradation and mineralization.[49] However, the process requires the synthesis of a new catalyst. In addition, the molecular catalyst was dissolved in the same solution as the PFAS making it difficult to separate the catalyst from the final fluorinated products.

Lithium metal-mediated degradation

When $LiClO_4$ is added as the salt and lithium metal is allowed to deposit, the degradation process is significantly enhanced by lithium-mediated electroreduction, LME (**Figure 3 (a-c)**). **Figure S3** shows that lithium metal is electrodeposited at these current densities as a shiny luster is present. Furthermore, the electrochemical profile shows the nucleation and growth overpotentials associated with lithium metal electrodeposition. As the ^{19}F NMR spectra in **Figure 3 (d)** shows, almost all the PFOA is converted to F^-. The degradation increases to 95% for PFOA and defluorination conversion up to 94 % (**Figure S4-5**). There are minute concentrations of TFA (trifluoroacetate) and no other smaller chain fluorinated compounds. Ion chromatography (IC) analysis identified formate as another degradation product, with no other detectable products observed (**Supplementary Note 4, Figure S6-8**).

For simplicity and future scalability, we use a single chamber membraneless cell. To demonstrate that PFOA is the sole source of fluorine in the reaction, it was conducted in the absence of any other potential fluorine sources, such as PTFE stir bars or Teflon-coated electrodes. **Figure S9** illustrates the degradation of PFOA and the formation of LiF both in the electrolyte and on the electrode surface, confirming that PFOA degradation is the exclusive source of fluoride ions. However, there is a need to clearly show that it is the lithium metal and the reductive process that leads to PFOA degradation and not oxidation. Therefore, we fabricated an H-Cell consisting of a Nafion cation exchange membrane to segregate the catholyte and anolyte chambers. **Figure S10-11** shows that the Nafion membrane can substantially limit PFOA and LiF crossover. When PFOA is added to the catholyte chamber, F^- is readily observed. In contrast, when PFOA is added to the anolyte chamber, F^- is not observed in the anolyte chamber, but only again in the catholyte chamber where we assume that some PFOA crossed over and degraded. Interestingly, regardless of whether PFOA was added to the catholyte or anolyte, LiF was observed on the surface of working electrode. This indicates that PFOA interacts with the Li surface, leading to the formation of LiF at the interface. For the single chamber experiments, we estimate the Coulombic efficiency (**Supplementary Note 3**) for PFOA degradation and conversion to fluorides in DMSO to be ~7.7%, which is higher than other reported electrochemical approaches (reductive or oxidative).[49, 50] To further improve this would involve optimization of the electrochemical cell, electrolyte composition, electrodes, and operating conditions.

The interfacial composition of the lithium metal and electrode surface was probed using XPS. For TBA-based electrolytes, the copper electrode was studied. **Figure 3 (e-g)** shows little/no degradation products on the copper surface for TBA indicating that the Cu doesn't participate directly in the reaction and serves primarily as a shuttle for electrons. All the fluorinated degradation products such as TBA-F are known to have high solubilities in organic media and are not present on the electrode surface but only in solution (see NMR data, **Figure S12**). In contrast, the electrodeposited lithium shows breakdown and defluorination of PFOA to F^- on the surface, mirroring some of the observations made in the proof-of-concept.

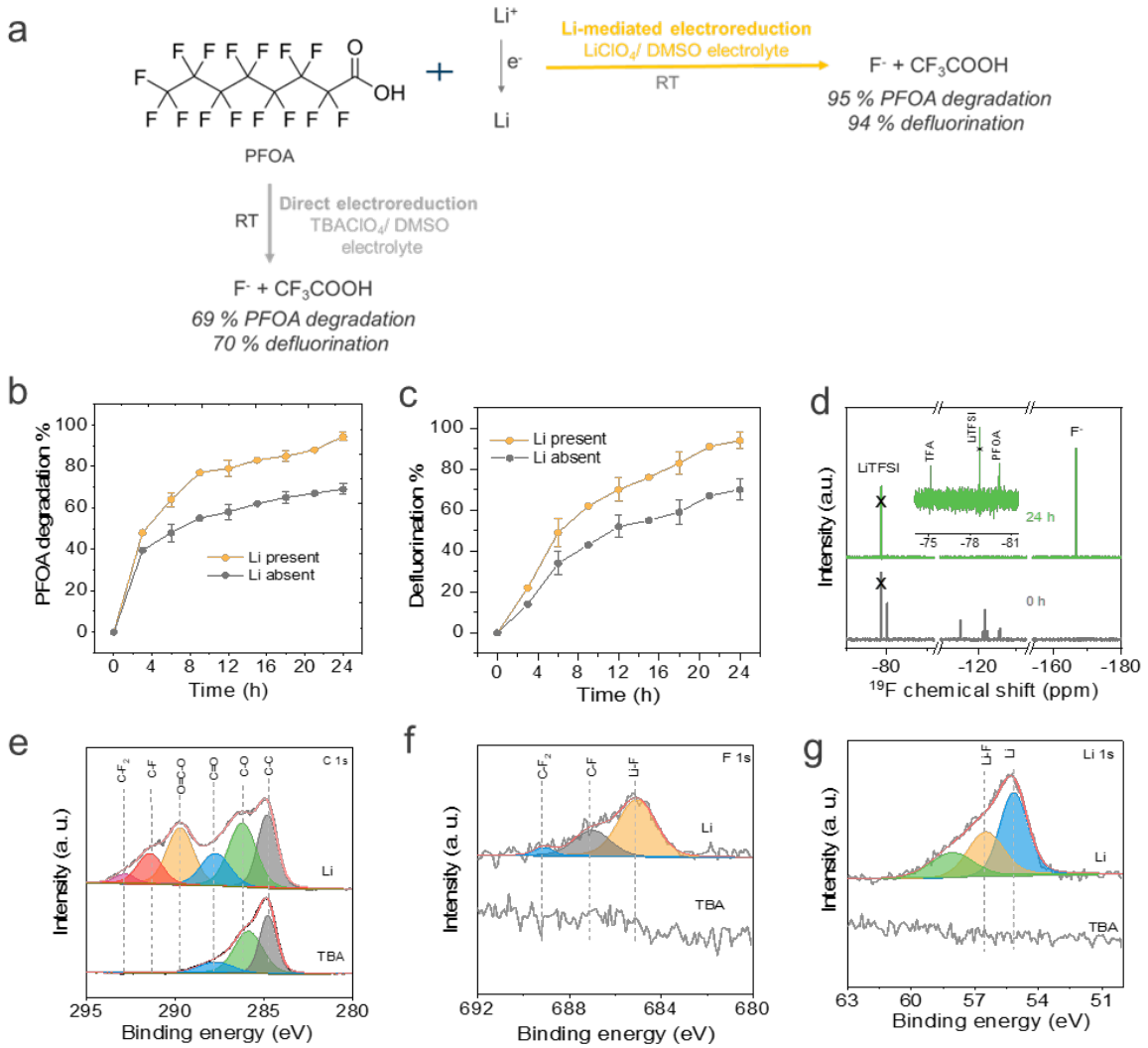

Fig 3. **Role of negative bias and Li in PFOA degradation** (**a**) Schematic of the degradation in presence and absence of Li, (**b**) PFOA degradation in presence (0.5 M $LiClO_4$) and absence of Li (0.5 M $TBAClO_4$) in DMSO with time at applied current density of 50 mA/cm^2, (**c**) Defluorination (fluoride recovery) with time, (**d**) ^{19}F NMR showing almost complete PFOA degradation, inset: depicting the trace amount of PFOA left and the formation of TFA as product, XPS data of (**e**) C 1s, (**f**) F 1s, and (**g**) Li 1s for TBA vs Li system.

Probing electrochemical reaction space

The influence of electrochemical variables such as current density, electrolyte, and electrode was further explored. The influence of reductive current on PFOA degradation was studied by varying the applied current density from 10 to 50 mA/cm^2 (**Figure S13**). As **Figure 4(a)** shows, current density plays an important role in the PFOA degradation. Even current densities as low as 10 mA/cm^2 show mineralization to F^- while the degradation at 40 mA/cm^2 largely mirrors that at 50 mA/cm^2. The ^{19}F NMR analysis reveals a progressive increase in the formation of LiF as a product, accompanied by a reduction in PFOA concentration (**Figure 4 (b)**). The reaction follows a pseudo first order reaction (**Supplementary note 5, Figure 4 (c)**) with a rate constant of 0.096 h^{-1}. An important observation for the degradation reactions in DMSO across all these current densities is that no smaller chain fluorinated residues are observed (which are typically reported in thermal and oxidative pathways).[51-53] Since the total amount of time is fixed while the current density varies, the amount of charge varies (**Figure S14**). As the total amount of charge applied increases, the PFOA degradation extent increases as shown in **Figure 4 (d)**. At the same fixed charge, there do appear to be differences in degradation extents, which we attribute to differences in the observed voltages. The influence of the anode was also studied with platinum and graphite showing similar overall cell voltages and no effect on the overall degradation (**Figure S15**). The anodic reaction was not optimized and is currently solvent oxidation. Future work can incorporate water for anodic oxygen evolution reaction (OER) or use a boron doped diamond (BDD) electrode to enable simultaneous reductive and oxidative PFAS destruction. It has been widely reported that electrolyte selection plays an important role in controlling lithium metal deposition efficiency, morphology, interfacial composition and more.[21, 54-57] Therefore, the influence of electrolyte selection on the electrochemical degradation process was explored. **Figure 4 (e)** shows that there is a significant electrolyte dependence, with PC showing the poorest degradation efficiencies while the EC: DG mixture is much closer to the DMSO-based system.

We also fabricated lithium metal batteries using these electrolytes to probe their influence on lithium metal CE (**Supplementary Note 5**). As **Figure S16** qualitatively shows, electrolytes that support low Li metal CE have higher PFOA degradation efficiencies. Although we do not want solvent competition with PFOA, we also do not want excellent electrolytes. These findings upend the heuristics for lithium metal batteries; hence electrolytes that have been discarded due to poor battery cycling – of which there are a multitude – can be resurrected for reactive metal degradation reactions. The influence of electrolyte selection on the lithium metal deposition morphology was also probed. **Figure 4 (f-k)** shows SEM images of lithium deposited at different current densities and with different electrolytes. In DMSO, the SEM of the samples reveal decrease in Li particle size with increasing current (**Figure 4 (f-h)).** As expected, the deposited lithium is highly porous with large active surface area for reaction with PFOA.

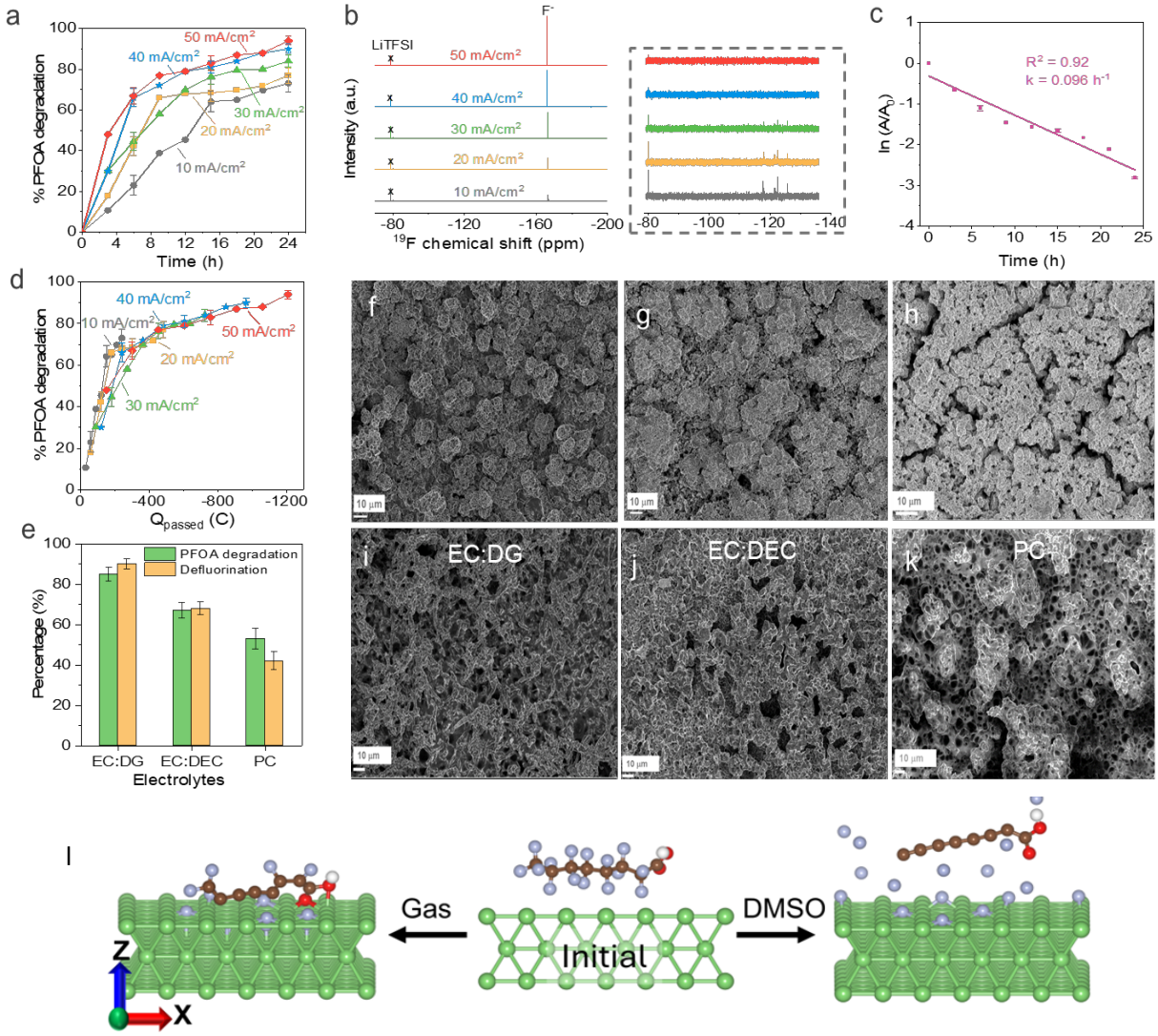

Fig. 4. Effect of reaction parameters on PFOA degradation. (**a**) Influence of current density on degradation of PFOA, (**b**) ^{19}F NMR showing PFOA degradation after 24 h at different current densities, selected region is zoomed 50x , (**c**) Plot of ln ([A/A$_0$]) vs. time where A$_0$ is the starting PFOA conc. (1 mM) and A is the conc. at time=t for a reaction carried out in DMSO at 50 mA/cm^2, SEM of electrodeposited Li at different J in DMSO, (**d**) Variation of degradation of PFOA with amount of charge passed, (**e**) influence of electrolyte selection, (**f**) 10 mA/cm^2, (**g**) 30 mA/cm^2 (**h**) 50 mA/cm^2. SEM of electrodeposited Li in different electrolytes at J = 50 mA/cm^2 (**i**) ethylene carbonate: diglyme (EC: DG), (**j**) ethylene carbonate: diethyl carbonate (EC: DEC), (**k**) propylene carbonate (PC). All depositions for SEM are done at a constant capacity of 2 mAh/cm^2. (**l**) Degradation of PFOA molecule near a Li surface in DMSO implicit solvents and in the gas phase, as determined by DFT calculations.

DFT investigation to understand degradation mechanism

Density functional theory (DFT) was performed to garner mechanistic insight into the degradation process (**Supplementary Note 7**). The calculations refer to PFOA near a small lithium crystal – Li (110) – in the presence of solvents whose influence is treated implicitly, and with all atoms free to move except for the Li's which are assumed fixed. The geometry of the PFOA molecule that is obtained from energy minimization of the starting structure is shown in **Figure 4 (l) and S18**. **Figure 4 (l)** shows significant fragmentation of the PFOA, with the results significantly altered in some solvent environments compared to others (**Figure S19**). In DMSO (dielectric constant (ε) ≈ 46.7), PC (≈ 64), and EC (≈ 89.78), the PFOA molecule is pushed away from the Li surface during the geometry relaxation process, with all C-F bonds degraded and the carbon chain becoming linear. The carbon chain structures are similar to the known structures of small anionic polyacetylenic carbon clusters with the same number of atoms,[58, 59] although in this case the carboxylate group (which has a Bader charge of 1.24 e) is not dissociated from the chain. In contrast, in low dielectric constant solvents, DG (≈ 7.2) and DEC (≈ 2.805), and in the gas phase, the PFOA molecule is attracted to the Li surface, and only roughly half of the C-F bonds are broken (**Figure S19**). To understand this behavior, the charge transfer dynamics was analyzed in both the gas phase and DMSO solvent systems. The results show (**Figure S19**) that the number of electrons transferred (ΔQ) is significantly higher when PFOA is solvated in DMSO, with 15.8 electrons transferred from the Li surface to the PFOA molecule, while the gas phase charge transfer is ~ 12.0 electrons. For both DMSO and vacuum, the high number of electrons transferred leads to substantial C-F bond degradation, but only DMSO result leads to complete defluorination, similar to the experimental observations. While this model is oversimplified compared to the experiment, these calculations suggest the conditions needed to remove all fluorines from PFOA. Note that the transfer of ~16 electrons to PFOA and degradation of 12 F^- leave the carbon fragment negatively charged such that it is repelled by F^- near the Li surface. Also, many of the F^- end up solvated in the DMSO, while others enter the lattice.

The effects of other solvent environments were investigated, including PC, DEC, EC, and DG. In the PC and EC solvents, we observed similar 100% C-F bond degradation, with charge transfers of 19.5 e and 17.0 e, respectively. These solvents, like DMSO, have relatively high dielectric constants, which likely contribute to the efficient charge transfer and subsequent C-F bond degradation. In the DEC and DG solvents, the lower dielectric constants lead to less stabilization of charged intermediates, less charge transfer and bond degradation. In DEC, we observed a lower C-F bond degradation fraction of 53.3%, with the corresponding charge transfer is 10.1 e. In DG, the C-F bond degradation fraction is 73.3%, similar to the gas phase, with a charge transfer of 13.9 e.

Overall, the DFT results show that these solvents are capable of supporting PFOA degradation to some extent, but only allow DMSO, PC, and EC allow for complete degradation. The superior performance of DMSO compared to the other solvents must therefore be interpreted in terms of the other factors mentioned earlier (solubility of LiF and Li porosity) that are not included in our modeling.

AIMD studies to understand the effect of electric field

To simulate the influence of an applied electrochemical potential on PFOA degradation, AIMD simulations were conducted at 0 K for 5 ps with and without an electric field perpendicular to a Li surface. The simulations aimed to understand the degradation mechanisms under different electric field conditions, specifically under a +0.5 eV/Å (reductive environment) and a -0.5 eV/Å (oxidative environment) electric field in DMSO solvent. Under a reductive environment (+0.5 eV/Å) in DMSO solvent, significant degradation was observed, with the breaking of eight C-F bonds and formation of Li-F bonds and F^- ions at 0.025 ps (**Figure S20 (a)**), and further bond degradations leading to a variety of fragments by 0.5 ps, similar to the energy-minimized result in **Figure 4(l)**. However, due to implicit solvent effects, only the short-term results (up to 0.0325 ps) are expected to be representative of actual experiments. The positive electric field enhances electron transfer from the Li surface to PFOA, corresponding to reductive conditions. The enhanced charge transfer (9.3 e) under the positive field correlates with higher PFOA defluorination (86.7%), accelerating degradation (**Figure S19 (b)**).

In contrast, a negative electric field (-0.5 eV/Å, oxidation) resulted in slower and less complete degradation, with bond breakages and fragment formation observed more gradually. This corresponds to oxidative conditions, where an oxidative process involves the loss of electrons from PFOA. Charge transfer from the Li surface to PFOA was lower (7.0 e) under the negative field, correlating with less defluorination (26.7%). The reduced rate of C-F bond degradation and fragmentation is consistent with the lower electron transfer to PFOA under these conditions.

The difference in degradation efficiency between positive and negative electric fields is attributed to charge transfer dynamics. The significant electronegativity difference between Li and PFOA atoms facilitates electron transfer from Li, weakening C-F bonds and promoting degradation. Under reductive conditions with a positive electric field, this process is more pronounced, leading to greater and faster PFOA degradation compared to oxidative conditions with a negative electric field.

Expanding reaction scope

Reactive metal mediated electrochemical reactions hold promise beyond lithium metal and beyond PFOA. Tackling the challenge of breaking down a wide variety of PFAS compounds requires methods that are both effective and versatile. Beyond the well-known PFAS like PFOA and GenX, the EPA has identified 40 PFAS across different structural categories.[60] These PFAS compounds are commonly found in wastewater, groundwater, soil, sediments, and fish tissue and EPA developed the popular Method 1633 to detect these 40 PFAS in various sources.

The application of the LME (lithium-mediated electroreduction) and DE (Direct Electroreduction) methods to these PFAS reveals promising trends. For perfluoroalkyl carboxylic acids ($C_nF_{(2n+1)}CO_2H$, where n = 3 to 12), both methods demonstrate greater degradation efficiency for longer-chain PFAS compared to shorter-chain ones (**Figure S21**). For example, the degradation is 99.1 % for PFUnA (n = 10) compared to 4 % for PFBA (n=3) as shown in Figure 5. This chain-length-dependent degradation has been observed in the literature, attributed to the more hydrophobic nature of longer-chain PFAS. Their increased hydrophobicity facilitates easier adsorption onto the reactive interface, in contrast to shorter-chain PFAS.[61, 62] Perfluorosulfonic acids, fluorotelomer carboxylic and sulfonic acids exhibit a similar trend, with higher degradation efficiencies observed for longer-chain PFAS.

Figure 5. **Scope of degradation**. Structures of PFAS belonging to different classes. The first value represents the degradation %, while the second indicates the defluorination % achieved using the LME and DE methods, respectively

Additionally, the LME method effectively degrades other PFAS classes, including perfluorooctane sulfonamide ethanols, sulfonamides, and per- and polyfluoroether carboxylic acids as shown in **Figure 5**. Notably, in all cases, the degradation percentage and defluorination efficiency achieved through LME consistently outperform those obtained with DE, highlighting the potential of LME for broader applicability and superior outcomes in PFAS mitigation efforts.

The modular nature of the process allows a different reactive metal to be studied if the relevant salt is available. Beyond lithium, we experimentally explored other reactive metals such as potassium by incorporating a potassium salt. **Figure S23** shows that K can enable 34 % degradation of PFOA to KF. Differences between Li and K primarily involve differences in the higher K electrolyte solution resistance (compared to Li) in the electrolytes studied here. Further optimization of the K-based electrolyte will be needed.

Valorization of degraded PFAS to non-PFAS product

The Department of Energy has listed fluorine as a critical element for energy; however, PFAS as discussed so far is a waste product. Therefore, recovering the fluorides obtained from PFAS degradation and converting them to non-PFAS fluorinated products can close the fluorine loop. We focus on KF since it has been reported widely as a reagent for fluorination reactions, and the synthesis of ethane sulfonyl fluoride (as an exemplar) because of its use in battery applications as well as in drug discovery. [37, 38] More importantly, ESF is not considered a PFAS by any definition. We first conduct the synthesis of ESF using commercial KF, following literature procedure for synthesizing sulfonyl fluorides (**Figure S24**).[63, 64] This served as a reference. After the degradation of PFOA, the resulting KF is separated from the DMSO

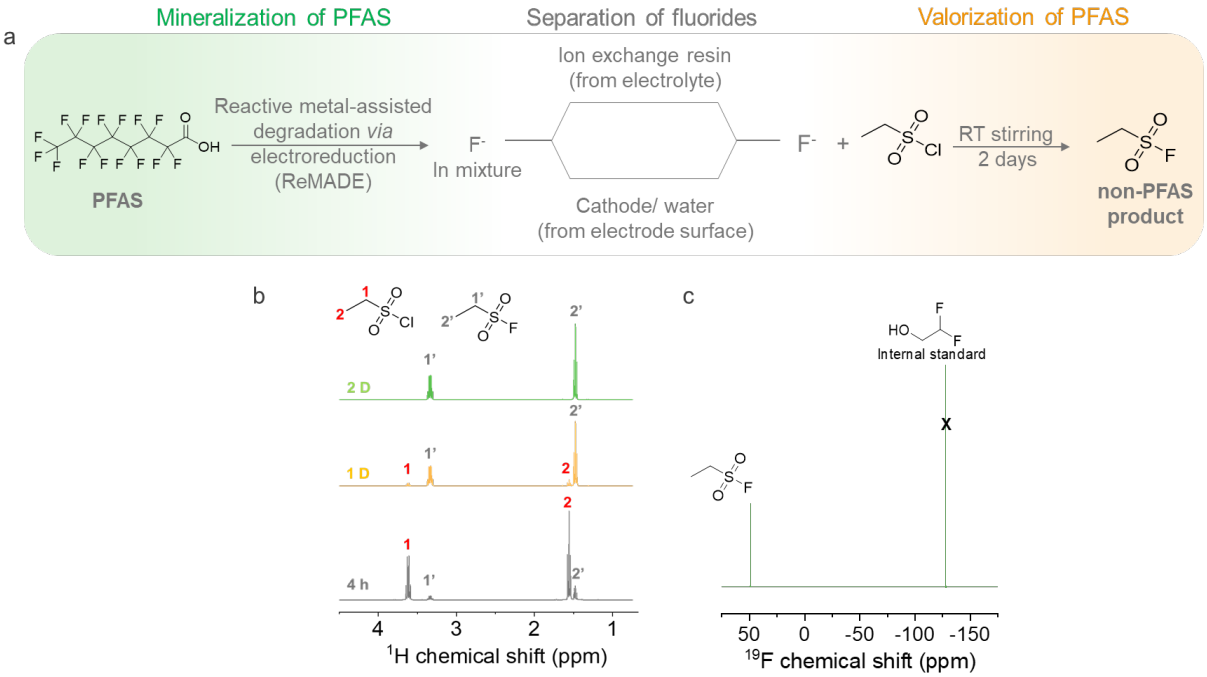

Figure 6. (a) Schematic showing the workflow from mineralization of PFAS to separation of fluorides and valorization to non-PFAS product, (b) 1H NMR depicting the formation of ESF from ESCl over 2 days (2 D), (c) 19F NMR showing formation of ESF and % yield after 2 D calculated with respect to 2, 2 difluoroethanol (denoted by x, internal standard).

electrolyte using multiple methods; either washing the cathode surface or ion exchange chromatography (**Figure 6(a), Figure S25, Supplementary note 9**). The collected fluoride is washed with water and concentrated using a rotary evaporator to obtain a saturated KF solution. This solution is then reacted with ethane sulfonyl chloride (ESCl), as a biphasic mixture. As shown in **Figure 6 (b)**, the ^{1}H NMR spectra reveal a gradual decrease in the ESCl peaks and a

corresponding increase in the ESF peaks, indicating the successful conversion of ESCl to ESF over two days. By the end of the reaction, only the ESF peak is observed with 82% yield (**Figure 6 (c)**). This process demonstrates a successful upcycling pathway, converting PFAS degradation products into ESF, a valuable non-PFAS fluorinated compound.

Our work on reactive metal-mediated electrochemical reactions provides an ambient temperature, pressure process that can take advantage of renewable electrons (solar, wind) in a modular manner. Future work will take advantage of other reactive metals (e.g., Na, Mg) with more positive reduction potentials (compared to Li) that have been shown in the battery literature to lead to defluorination. [65, 66] Furthermore, other compounds such as halogenated products (e.g., chloro-, bromo-) and polymers (e.g., chloro and fluoro-polymers) will be pursued. Finally, the confluence of reductive degradation and reactive metals enabled by careful electrolyte engineering changes the paradigm of electrochemical reactions ranging from electrocatalysis to electrosynthesis to environmental degradation.

Conclusions

A novel Li metal mediated electrochemical route was developed for PFOA degradation as part of a broader process we term ReMADE (reactive metal-assisted degradation reactive metal-assisted degradation *via* electroreduction). The ambient temperature, pressure, catalyst-free system led to up to 94 % defluorination of PFOA after 24 hours under highly reductive environment in DMSO. Notably, in the absence of Li, the degradation proceeds partially on a pristine Cu surface, which indicates that reductive conditions are important. LiF is the major degradation product and no shorter alkyl chain compounds were seen apart from trace amounts of TFA (trifluoroacetate). Increase in reductive current enhances the degradation due to improved availability of the Li active surface area with decrease in Li nucleation size. We show that electrolyte choice is important with DMSO supporting high defluorination and LiF solubility. DFT and AIMD results provide further insight and show that the degradation is associated with degradation of C-F bonds that occurs because of electron transfer from Li to the PFOA in DMSO, leaving behind F^-, LiF and a carboxylated carbon chain. We study the influence of lithium metal mediated degradation with other fluorinated compounds and show degradation. The degradation % achieved through LME consistently surpass those obtained with DE and out of the 33 PFAS tested, 22 demonstrated degradation exceeding 70%, with PFUnA and PFDA achieving a remarkable degradation of 99%. Furthermore, we explore other alkali metals such as potassium. Finally, we valorize the inorganic fluorides from PFOA degradation for the synthesis of fluorinated non-PFAS products. Inspired by the battery literature, we take the disadvantages that plague electrolyte development for reactive metal-based batteries and exploit them for desired halogenated compound degradation. Our findings are relevant for several electrochemical transformations such as electrocatalysis, electrosynthesis, and environmental remediation.

Materials and methods

PFOA (Perfluorooctanoic acid, 95 %), Lithium perchlorate (99%), dimethyl sulfoxide (anhydrous, 99.9%), ethylene carbonate (anhydrous, 98 %), diglyme (anhydrous, 99.5%), diethyl carbonate (99 %), propylene carbonate (anhydrous, 99 %), and 4 Å molecular sieves were purchased from Sigma-Aldrich. Gen X (95 %) is purchased from Sigma Aldrich and LiTFA (97 %) from Thermo Scientific. Tetrabutylammonium perchlorate (99 %) was purchased from Alfa Aesar. Ethane sulfonyl chloride (> 98 % purity) is purchased from TCI. Deuterated DMSO (≥ 99.8 atom % D) was purchased from Cambridge Isotope Laboratories. PFBA (Perfluorobutanoic acid), PFPeA (Perfluoropentanoic acid), PFHxA (Perfluorohexanoic acid), PFHpA (Perfluoroheptanoic acid), PFOA (Perfluorooctanoic acid), PFNA (Perfluorononanoic acid), PFDA (Perfluorodecanoic acid), PFUnA (Perfluoroundecanoic acid), PFTrDA (Perfluorotridecanoic acid), PFTeDA (Perfluorotetradecanoic acid), PFBS (Perfluorobutanesulfonic acid), PFHpS (Perfluoroheptanesulfonic acid),4:2 FTS (1H,1H,2H,2H-Perfluorobutane sulfonic acid), 6:2 FTS (1H,1H,2H,2H-Perfluorohexane sulfonic acid), 8:2 FTS (1H,1H,2H,2H-Perfluorooctane sulfonic acid), PFOSA (Perfluorooctane sulfonamide), NMeFOSA (N-Methyl perfluorooctane sulfonamide), NMeFOSE (N-Methyl perfluorooctane sulfonamidoethanol), PFMPA (Perfluoro-4-methoxypropanoic acid), PFMBA (Perfluoro-4-methoxybutanoic acid), NFDHA (Nonafluorodimethylhexane acid), 5:3 FTCA (5:3 Fluorotelomer carboxylic acid), 7:3 FTCA (7:3 Fluorotelomer carboxylic acid) were purchased from Sigma Aldrich. 9Cl-PF3ONS (9-Chlorohexadecafluoro-3-oxanonane-1-sulfonic acid), 1Cl-PF3OUdS (1-Chlorotridecafluoro-3-oxaundecane-1-sulfonic acid), PFEESA (Perfluoroethyl ethyl sulfonamide) were purchased from LGC standards. ADONA (4,8-Dioxa-3H-perfluorononanoic acid), 3:3 FTCA (3:3 Fluorotelomer carboxylic acid), NEtFOSE (N-Ethyl perfluorooctane sulfonamidoethanol), NMeFOSAA (N-Methyl perfluorooctane sulfonamidoacetic acid), PFPeS (Perfluoropentane sulfonic acid), PFHxS (Perfluorohexane sulfonic acid), PFOS (Perfluorooctane sulfonic acid), PFNS (Perfluorononane sulfonic acid), PFDS (Perfluorodecane sulfonic acid), PFDoS (Perfluorododecane sulfonic acid) were purchased from Cayman Chemicals. The different solvents were dried and stored with 4 Å molecular sieves overnight inside an Ar-filled glovebox (VigorTech, O_2 and H_2O < 1 ppm). All the PFAS and salts used were vacuum dried overnight before transferring to the glovebox. The Cu working electrode (0.28 cm^2, 99.99%) was purchased from McMaster-Carr and designed by taking the polycrystalline Cu rod and mounted into a PTFE tube. Ag/AgCl reference electrodes were purchased from eDAQ and graphite rod counter electrode was purchased from Sigma Aldrich.

Electrochemical characterization

All electrochemical characterizations were carried out using a Bio-Logic VSP-300 potentiostat inside an Ar-filled glovebox, utilizing a typical three-electrode polypropylene cell. The setup included a Cu rod (0.28 cm^2) as the working electrode, a leakless Ag/AgCl as the reference electrode, and a graphite rod as the counter electrode (**Figure S2**) at room temperature. The Cu electrode was soaked in a 0.1 M aqueous sulfuric acid solution for 30 minutes to remove any organic contaminants and passivation layer. It was then polished on a cloth pad with alumina suspension, rinsed with Milli-Q water (18.4 MΩ·cm), and sonicated for 15 minutes. Chronopotentiometry (CP) experiments were conducted at a constant applied current density ranging from 10 to 50 mA/cm^2 for 24 hours at room temperature with magnetic stirring at 400

rpm. The initial PFOA concentration was 1 mM with 0.5 M $LiClO_4$ or $TBAClO_4$ in 5 mL of DMSO, unless otherwise specified.

Nuclear magnetic resonance (NMR)

NMR spectra were recorded on a Bruker Ascend instrument (400 MHz) using a capillary setup inside a Wilmad NMR tube. An internal standard (2 mM LiTFSI) in deuterated DMSO was placed inside a capillary tube and capped with a PTFE cover. For analysis, 400 µL of the sample was used, and the capillary with the internal standard in DMSO-d6 was added.

X-ray photoelectron spectroscopy (XPS)

All the XPS measurements were carried out using the Physical Electronics, PHI 5000 VersaProbe II System equipped with an Al K*a* radiation (h*v* = 1,486.6 eV) beam (100 µm, 25 W). Cu foil (0.5*6 cm^2) is used as the working electrode for investigating XPS which is masked with tape to have an exposed surface area of 0.5*0.5 cm^2 immersed in the electrolyte. The electrodeposition of Li is done inside an Ar-filled glovebox. After electrodeposition, the area with Li deposition on the foil is cut and rinsed three times with dimethoxy ethane (DME) and transferred to a glass vial. The foil is dried in glovebox antechamber for 30 minutes under vacuum to get rid of any residual solvent. The data was fitted using CasaXPS software[67] with C-C peak in C 1s referenced at 284.8 eV.

Scanning electron microscopy (SEM)

SEM images are taken on a Carl Zeiss Merlin field emission SEM with an accelerating voltage of 15 kV. Cu foil is used as the working electrode to deposit Li (similar to sample preparation mentioned above for XPS). The deposition capacity for all the samples was fixed to 2 mAh/cm^2. After electrodeposition, the samples were washed with DME three times, transferred into a vial and moved to the glovebox antechamber for drying.

Ion chromatography (IC)

A Shimadzu LC-20Ai IC system consisting of a conductivity detector (CDD-10AVP) was used to obtain all ion chromatograms. 10 µL sample was injected into the column using an autosampler (SIL-20AC). Separations were carried out on an analytical column (Shodex IC NI-424, anion-specific) coupled with a guard column (Shodex IC IA-G). The column was maintained at 40°C, with a run time of 20 minutes. For optimal peak separation of various anions, two mobile phases were utilized. The first mobile phase consisted of 8 mM 4-Hydroxybenzoic acid, 1.9 mM Bis-Tris, 2 mM Phenylboronic acid, and 0.005 mM trans-1,2-Diaminocyclohexane-N, N, N', N'-tetraacetic acid in aqueous solution. The second mobile phase was identical, except for the exclusion of Bis-Tris. Data collection and processing were performed using the LabSolutions software.

Gas chromatography mass spectrometry (GCMS)

A Shimadzu GCMS-QP2020 NX single quadrupole mass spectrometer, equipped with an HS-20 Headspace autosampler, was employed to analyze post-degradation samples. Separation was achieved using an SH-Q-BOND column (30 m × 0.32 mm × 10 µm) with helium as the carrier gas. The detector temperature was maintained at 40 °C, and 1 mL of undiluted sample was used for analysis.

Liquid chromatography mass spectrometry (LCMS)

LCMS data was collected using a Shimadzu Nexera LC-40DXR UHPLC coupled with a LCMS-2050 single quadrupole detector. Separation was carried out with two mobile phases: mobile phase A consisted of acetonitrile, while mobile phase B was 5 mM aqueous ammonium acetate. A Shimadzu Nexcol C18 column (1.8 µm, 50 × 2.1 mm) was used for the separation, with an Agilent Eclipse Plus C18 guard column (1.8 µm, 3 × 5 mm). The column temperature was maintained at 40 °C. Samples were diluted to a total volume of 500 µL using a 1:1 mixture of water and acetonitrile, with 5 µL of injection volume for each run.

Conflicts of Interest

There are no conflicts of interest to declare.

Acknowledgments

This work was supported by the Advanced Materials for Energy-Water Systems (AMEWS) Center, an Energy Frontier Research Center funded by the U.S. Department of Energy, Office of Science, Basic Energy Sciences under Contract No. DE-AC02-06CH11357. The GCMS used in this research was also supported by the AMEWS EFRC. Computational research was supported in part through the Quest high-performance computing facility at Northwestern University. The authors also thank Northwestern University for its support. SEM was done at the shared facility at the University of Chicago Materials Research Science and Engineering Center (MRSEC), supported by the National Science Foundation under award number DMR-2011854. NMR was performed at the UChicago Chemistry NMR facility.

References

1. J. Glüge, M. Scheringer, I. T. Cousins, J. C. DeWitt, G. Goldenman, D. Herzke, R. Lohmann, C. A. Ng, X. Trier and Z. Wang, *Environmental Science: Processes & Impacts*, 2020, **22**, 2345-2373.
2. S. E. Fenton, A. Ducatman, A. Boobis, J. C. DeWitt, C. Lau, C. Ng, J. S. Smith and S. M. Roberts, *Environmental Toxicology and Chemistry*, 2021, **40**, 606-630.
3. J. J. Shearer, C. L. Callahan, A. M. Calafat, W.-Y. Huang, R. R. Jones, V. S. Sabbisetti, N. D. Freedman, J. N. Sampson, D. T. Silverman, M. P. Purdue and J. N. Hofmann, *JNCI: Journal of the National Cancer Institute*, 2020, **113**, 580-587.
4. What are the health effects of PFAS?, https://www.atsdr.cdc.gov/pfas/health-effects/index.html).
5. *EPA - Final PFAS National Primary Drinking Water Regulation*, 2024.
6. Y. Wang, S. B. Darling and J. Chen, *ACS Applied Materials & Interfaces*, 2021, **13**, 60789-60814.
7. R. F. Menger, E. Funk, C. S. Henry and T. Borch, *Chemical Engineering Journal*, 2021, **417**, 129133.
8. B. Cantoni, A. Turolla, J. Wellmitz, A. S. Ruhl and M. Antonelli, *Science of The Total Environment*, 2021, **795**, 148821.
9. F. Dixit, R. Dutta, B. Barbeau, P. Berube and M. Mohseni, *Chemosphere*, 2021, **272**, 129777.
10. L. Xiao, C. Ching, Y. Ling, M. Nasiri, M. J. Klemes, T. M. Reineke, D. E. Helbling and W. R. Dichtel, *Macromolecules*, 2019, **52**, 3747-3752.
11. J. N. Meegoda, B. Bezerra de Souza, M. M. Casarini and J. A. Kewalramani, *Journal*, 2022, **19**.
12. Y. Wu, Y. Li, C. Fang and C. Li, *ChemCatChem*, 2019, **11**, 2297-2303.
13. N. B. Üner, P. Baldaguez Medina, J. L. Dinari, X. Su and R. M. Sankaran, *Langmuir*, 2022, **38**, 8975-8986.

14. https://epa.gov/pfas).
15. Y. Li, N. Che, N. Liu and C. Li, *Chemical Engineering Journal*, 2023, **478**, 147443.
16. J. N. Uwayezu, I. Carabante, T. Lejon, P. van Hees, P. Karlsson, P. Hollman and J. Kumpiene, *Journal of Environmental Management*, 2021, **290**, 112573.
17. C. E. Schaefer, C. Andaya, A. Burant, C. W. Condee, A. Urtiaga, T. J. Strathmann and C. P. Higgins, *Chemical Engineering Journal*, 2017, **317**, 424-432.
18. R. Bansal, R. Verduzco, M. S. Wong, P. Westerhoff and S. Garcia-Segura, *Journal of Electroanalytical Chemistry*, 2022, **907**, 116028.
19. M. Bolloli, J. Kalhoff, F. Alloin, D. Bresser, M. L. Phung Le, B. Langlois, S. Passerini and J.-Y. Sanchez, *The Journal of Physical Chemistry C*, 2015, **119**, 22404-22414.
20. Y. Wang, Z. Wu, F. M. Azad, Y. Zhu, L. Wang, C. J. Hawker, A. K. Whittaker, M. Forsyth and C. Zhang, *Nature Reviews Materials*, 2024, **9**, 119-133.
21. P. Ma, P. Mirmira and C. V. Amanchukwu, *ACS Central Science*, 2021, **7**, 1232-1244.
22. P. Ma, P. Mirmira, P. J. Eng, S.-B. Son, I. D. Bloom, A. S. Filatov and C. V. Amanchukwu, *Energy & Environmental Science*, 2022, **15**, 4823-4835.
23. D. T. Boyle, W. Huang, H. Wang, Y. Li, H. Chen, Z. Yu, W. Zhang, Z. Bao and Y. Cui, *Nature Energy*, 2021, **6**, 487-494.
24. Y. Zhao, T. Zhou, T. Ashirov, M. E. Kazzi, C. Cancellieri, L. P. H. Jeurgens, J. W. Choi and A. Coskun, *Nature Communications*, 2022, **13**, 2575.
25. Y. Rao, X. Li, S. Zhao, P. Liu, F. Wu, X. Liu, N. Zhou, S. Fang and S. Passerini, *Nano Energy*, 2024, **123**, 109362.
26. S.-J. Park, J.-Y. Hwang, C. S. Yoon, H.-G. Jung and Y.-K. Sun, *ACS Applied Materials & Interfaces*, 2018, **10**, 17985-17993.
27. P. Ma, R. Kumar, M. C. Vu, K.-H. Wang, P. Mirmira and C. V. Amanchukwu, *Journal of Materials Chemistry A*, 2024, **12**, 2479-2490.
28. B. H. R. Suryanto, K. Matuszek, J. Choi, R. Y. Hodgetts, H.-L. Du, J. M. Bakker, C. S. M. Kang, P. V. Cherepanov, A. N. Simonov and D. R. MacFarlane, *Science*, 2021, **372**, 1187-1191.
29. K. Steinberg, X. Yuan, C. K. Klein, N. Lazouski, M. Mecklenburg, K. Manthiram and Y. Li, *Nature Energy*, 2023, **8**, 138-148.
30. M. J. Bentel, Y. Yu, L. Xu, Z. Li, B. M. Wong, Y. Men and J. Liu, *Environmental Science & Technology*, 2019, **53**, 3718-3728.
31. S. Biswas, X. Wang and B. M. Wong, *Current Opinion in Chemical Engineering*, 2024, **44**, 101017.
32. J. F. King and B. P. Chaplin, *Current Opinion in Chemical Engineering*, 2024, **44**, 101014.
33. H. K. Liberatore, S. R. Jackson, M. J. Strynar and J. P. McCord, *Environmental Science & Technology Letters*, 2020, **7**, 477-481.
34. B. Trang, Y. Li, X.-S. Xue, M. Ateia, K. N. Houk and W. R. Dichtel, *Science*, 2022, **377**, 839-845.
35. J. Zhu, Y. Chen, Y. Gu, H. Ma, M. Hu, X. Gao and T. Liu, *Journal of Hazardous Materials*, 2022, **422**, 126953.
36. 2023 DOE Critical Materials List, https://www.iea.org/policies/17976-2023-doe-critical-materials-list).
37. K. S. Jiang, G. M. Hobold, R. Guo, K.-H. Kim, A. M. Melemed, D. Wang, L. Zuin and B. M. Gallant, *ACS Energy Letters*, 2022, **7**, 3378-3385.
38. C. V. M. Kumar R, Ma P, Amanchukwu C. , *ChemRxiv. 2024; doi:10.26434/chemrxiv-2024-vqtc7 This content is a preprint and has not been peer-reviewed.*
39. S. Wei, Z. Li, K. Kimura, S. Inoue, L. Pandini, D. Di Lecce, Y. Tominaga and J. Hassoun, *Electrochimica Acta*, 2019, **306**, 85-95.
40. M. Morita, F. Tachihara and Y. Matsuda, *Electrochimica Acta*, 1987, **32**, 299-305.
41. Y. Xie, H. Xiang, P. Shi, J. Guo and H. Wang, *Journal of Membrane Science*, 2017, **524**, 315-320.

42. A. J. Louli, A. Eldesoky, R. Weber, M. Genovese, M. Coon, J. deGooyer, Z. Deng, R. T. White, J. Lee, T. Rodgers, R. Petibon, S. Hy, S. J. H. Cheng and J. R. Dahn, *Nature Energy*, 2020, **5**, 693-702.
43. Y. Yamada, K. Furukawa, K. Sodeyama, K. Kikuchi, M. Yaegashi, Y. Tateyama and A. Yamada, *Journal of the American Chemical Society*, 2014, **136**, 5039-5046.
44. F. Zhao, Z. Jing, X. Guo, J. Li, H. Dong, Y. Tan, L. Liu, Y. Zhou, R. Owen, P. R. Shearing, D. J. L. Brett, G. He and I. P. Parkin, *Energy Storage Materials*, 2022, **53**, 638-645.
45. Y. Gao, T. Rojas, K. Wang, S. Liu, D. Wang, T. Chen, H. Wang, A. T. Ngo and D. Wang, *Nature Energy*, 2020, **5**, 534-542.
46. L. Sun, C. Peng, L. Kong, Y. Li and W. Feng, *ENERGY & ENVIRONMENTAL MATERIALS*, 2023, **6**, e12323.
47. N. Xin, Y. Sun, M. He, C. J. Radke and J. M. Prausnitz, *Fluid Phase Equilibria*, 2018, **461**, 1-7.
48. J. Jones, M. Anouti, M. Caillon-Caravanier, P. Willmann and D. Lemordant, *Fluid Phase Equilibria*, 2009, **285**, 62-68.
49. S. Sinha, A. Chaturvedi, R. K. Gautam and J. J. Jiang, *Journal of the American Chemical Society*, 2023, **145**, 27390-27396.
50. C. E. Schaefer, S. Choyke, P. L. Ferguson, C. Andaya, A. Burant, A. Maizel, T. J. Strathmann and C. P. Higgins, *Environmental Science & Technology*, 2018, **52**, 10689-10697.
51. N. H. Weber, L. J. Dixon, S. P. Stockenhuber, C. C. Grimison, J. A. Lucas, J. C. Mackie, M. Stockenhuber and E. M. Kennedy, *Chemical Engineering Science*, 2023, **278**, 118924.
52. F. Xiao, P. C. Sasi, B. Yao, A. Kubátová, S. A. Golovko, M. Y. Golovko and D. Soli, *Environmental Science & Technology Letters*, 2020, **7**, 343-350.
53. S. Barisci and R. Suri, *Chemosphere*, 2020, **243**, 125349.
54. S. Ko, T. Obukata, T. Shimada, N. Takenaka, M. Nakayama, A. Yamada and Y. Yamada, *Nature Energy*, 2022, **7**, 1217-1224.
55. G. M. Hobold, C. Wang, K. Steinberg, Y. Li and B. M. Gallant, *Nature Energy*, 2024, **9**, 580-591.
56. C. V. Amanchukwu, Z. Yu, X. Kong, J. Qin, Y. Cui and Z. Bao, *Journal of the American Chemical Society*, 2020, **142**, 7393-7403.
57. Z. Yu, P. E. Rudnicki, Z. Zhang, Z. Huang, H. Celik, S. T. Oyakhire, Y. Chen, X. Kong, S. C. Kim, X. Xiao, H. Wang, Y. Zheng, G. A. Kamat, M. S. Kim, S. F. Bent, J. Qin, Y. Cui and Z. Bao, *Nature Energy*, 2022, **7**, 94-106.
58. G. von Helden, P. R. Kemper, N. G. Gotts and M. T. Bowers, *Science*, 1993, **259**, 1300-1302.
59. J. M. L. Martin and P. R. Taylor, *The Journal of Physical Chemistry*, 1996, **100**, 6047-6056.
60. Clean Water Act Analytical Methods - EPA, https://www.epa.gov/cwa-methods/cwa-analytical-methods-and-polyfluorinated-alkyl-substances-pfas#method-1633).
61. N. Loganathan and A. K. Wilson, *Environmental Science & Technology*, 2022, **56**, 8043-8052.
62. T. Shende, G. Andaluri and R. Suri, *Chemical Engineering Journal Advances*, 2023, **15**, 100509.
63. W. Davies and J. H. Dick, *Journal of the Chemical Society (Resumed)*, 1932, DOI: 10.1039/JR9320000483, 483-486.
64. R. Alan Aitken, M. J. Drysdale, G. Ferguson and A. J. Lough, *Journal of the Chemical Society, Perkin Transactions 1*, 1998, DOI: 10.1039/A707948F, 875-880.
65. Q. Yi, Y. Lu, X. Sun, H. Zhang, H. Yu and C. Sun, *ACS Applied Materials & Interfaces*, 2019, **11**, 46965-46972.
66. X. Zheng, Z. Gu, X. Liu, Z. Wang, J. Wen, X. Wu, W. Luo and Y. Huang, *Energy & Environmental Science*, 2020, **13**, 1788-1798.
67. N. Fairley, V. Fernandez, M. Richard-Plouet, C. Guillot-Deudon, J. Walton, E. Smith, D. Flahaut, M. Greiner, M. Biesinger, S. Tougaard, D. Morgan and J. Baltrusaitis, *Applied Surface Science Advances*, 2021, **5**, 100112.